Neural Network Modeling on Bioconvection Flow Subjected to the Magnetic Source

Ezgi Kiratli[1], Merve Gurbuz-Caldag[2] and Bengisen Pekmen[3]

Abstract— In this study, neural network modeling on a bioconvection flow problem is utilized. The data is collected from the numerical computations. The dimensionless governing equations of Cu-water nanofluid flow in a square cavity involving oxytactic bacteria under the effect of a magnetic source are numerically solved by radial basis function collocation method. In various values of Rayleigh, bioconvection Rayleigh, Peclet, Hartmann, magnetic numbers and coordinates of location of magnetic source, an iterative system is executed, and the outputs, average Nusselt and Sherwood numbers, density and the mean of bacteria are stored with the associated computed parameter values. The dataset of size 3645×11 created by this way is used for neural network modeling. The different train-test set sizes as well as the number of hidden layers, the layer sizes are controlled. In the light of mean squared error metric results, the obtained models show that the one layer neural network using small number of neurons also give good results. These models allow one to get prompt results instead of many times repeated numerical calculations.

I. INTRODUCTION

Bioconvection is the convective motion of a fluid resulting from the directional swimming of microorganisms in the presence of gravity, magnetic field, oxygen or light. Bioconvection has a wide range of applications including bio-microsystems, enzyme-based biosensors, photobioreactors, the food industry, mass transit augmentation, oil recovery systems and mixing processes [1]. Hillesdon and Pedley [2] conducted a linear instability analysis of the steady-state cell and oxygen concentration distributions. Kuznetsov [3] utilized Galerkin method to examine the thermo-bioconvection of oxytactic bacteria in a porous medium. The impact of oxytactic bacteria on the bioconvection flow nanofluid saturated porous square cavity is considered by Balla et al. [4]. It is reported that heat transfer rate increases as Peclet and Lewis numbers rise. Magnetic field effect on the heat and mass transfer of the bioconvection flow is examined including Lorentz force terms into the governing equations. Biswas et al. [5], [6], [7] depicted the influence of horizontally applied magnetic field on the convection flow including oxytactic bacteria in two-sided lid-driven square cavities, and the enclosure with a bell-shaped curved bottom wall. Hussain and Pekmen Geridonmez [8] implemented finite element method to investigate the influence of periodic magnetic field on Ag-MgO/water hybrid nanofluid in a porous medium inside a right trapezoidal cavity including oxytactic bacteria. It is obtained that periodic magnetic field weakens the convective heat and mass transfer.

Machine learning algorithms on bioconvection problems are conducted by many researchers. In [9], the Sherwood number (Sh), motile density of microorganism, skin friction coefficient and Nusselt number (Nu) are predicted using four different artificial neural network models. Chandra and Das [10] developed artificial neural network (ANN) model for the estimation of nanofluid flow over a stretchable vertically inclined surface containing gyratactic bacteria. Hussain et al. [11] proposed a support vector machine model for the bioconvection flow in the presence of magnetic field and oxytactic bacteria using data gathered from Galerkin finite element method. In [12], the average Nu, Sh and motile microorganism numbers of the mixed bioconvection flow of nanofluid of oxytactic bacteria through a porous cavity under the effect of periodic magnetic field is modeled using Light Gradient Boosting Machine algorithm. Rehman et al. [13] implemented the Levenberg-Marquardt scheme with a backpropagation NN to forecast Nu for bioconvection problem. Sait et al. [14] compared AI tools for the estimation of boundary layer flow for bioconvection subjected to the magnetic field.

In this study, NN modeling on a bioconvection flow in a square cavity filled by Cu-water nanofluid in the presence of oxytactic bacteria is conducted. To the best of authors' knowledge, the impact of magnetic source on the heat and mass transfer of bioconvection flow is firstly taken into account. The location of the magnetic source is also included in the NN process as an input variable. In the following parts, the physics of the problem, computational approaches, modeling results and conclusion are presented.

II. PHYSICS OF THE PROBLEM

Under steady-state conditions, natural convection flow of Cu-water nanofluid in a square cavity, taking into account the presence of oxytactic bacteria and the influence of a magnetic source is concerned. The setup of the problem is illustrated in Fig. 1. The location of magnetic source (ms) is denoted by (x_{ms}, y_{ms}).

*This work was not supported by any organization

[1]Ezgi Kiratli is with the Department of Economics, TED University, Ankara, 06420, Turkey ezgi.kiratli@tedu.edu.tr

[2]Merve Gurbuz-Caldag is with the Department of Mathematics, TED University, Ankara, 06420, Turkey merve.gurbuz@tedu.edu.tr

[3]Bengisen Pekmen is with the Department of Mathematics, TED University, Ankara, 06420 , Turkey bengisen.pekmen@tedu.edu.tr

The single-phase model is adopted for the nanofluid, and accordingly, its physical properties are defined by [15]

$$\rho_{nf} = (1-\xi)\rho_f + \xi\rho_s, \tag{1}$$
$$(\rho c_p)_{nf} = (1-\xi)(\rho c_p)_f + \xi(\rho c_p)_s, \tag{2}$$
$$(\rho\beta)_{nf} = (1-\xi)(\rho\beta)_f + \xi(\rho\beta)_s, \tag{3}$$
$$\alpha_{nf} = \frac{k_{nf}}{(\rho c_p)_{nf}}, \tag{4}$$

where subindices nf, f, s are the nanofluid, fluid and solid, respectively, ρ is the density, β is the thermal expansion coefficient, c_p is the specific heat, α is the thermal diffusivity and ξ is the solid volume fraction. The thermal (k_{nf}) and electrical σ_{nf} conductivities of the nanofluid are settled as [16]

$$\frac{k_{nf}}{k_f} = \frac{k_s + 2k_f - 2\xi(k_f - k_s)}{k_s + 2k_f + \xi(k_f - k_s)}, \tag{5}$$
$$\frac{\sigma_{nf}}{\sigma_f} = \frac{\sigma_s + 2\sigma_f - 2\xi(\sigma_f - \sigma_s)}{\sigma_s + 2\sigma_f + \xi(\sigma_f - \sigma_s)}, \tag{6}$$

and the dynamic viscosity of nanofluid μ_{nf} is opted as [17]

$$\mu_{nf} = \mu_f(1-\xi)^{-2.5}. \tag{7}$$

Table I summarizes the thermophysical properties of water and copper (Cu).

TABLE I
Thermophysical properties of water and Copper (Cu) [5], [18]

Property	Water	Cu
$\rho\ (kg/m^3)$	997.1	8933
$c_p\ [J/(kgK)]$	4179	385
$k\ [W/(mK)]$	0.613	401
$\beta \times 10^{-5}\ (1/K)$	21	1.67
$\sigma\ (1/(m\Omega))$	0.05	5.96×10^7

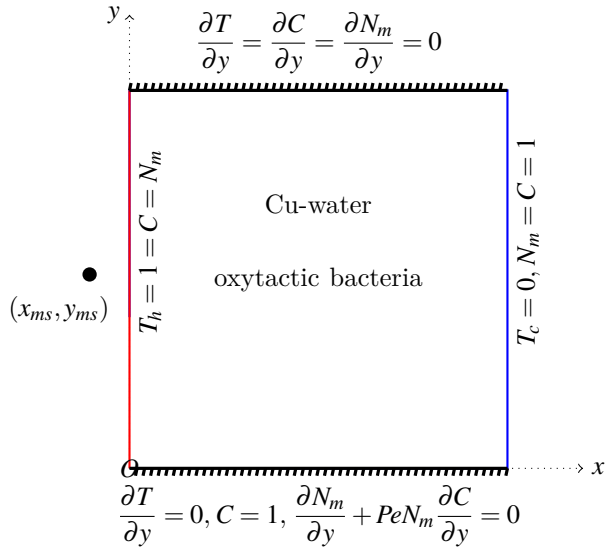

Fig. 1. The geometrical layout of the problem.

By using the stream function to define the velocity components, $\nabla\cdot(u,v) = 0$ is satisfied. Additionally, introducing vorticity eliminates the pressure terms from the momentum equations. As a result, the governing equations are reformulated in terms of stream function (ψ), vorticity (ω), temperature (T), oxygen concentration (C) and the density of the bacteria (N_m) as follows:

$$\nabla^2\psi = -\omega, \tag{8a}$$
$$\frac{\alpha_{nf}}{\alpha_f}\nabla^2 T = \left(u\frac{\partial T}{\partial x} + v\frac{\partial T}{\partial y}\right), \tag{8b}$$
$$\frac{1}{Le}\nabla^2 C = \left(u\frac{\partial C}{\partial x} + v\frac{\partial C}{\partial y}\right) + \frac{1}{Le}N_m, \tag{8c}$$
$$\frac{1}{Le}\nabla^2 N_m = \left(u\frac{\partial N_m}{\partial x} + v\frac{\partial N_m}{\partial y}\right) + \frac{Pe}{Le}\left(N_m\nabla^2 C + \frac{\partial C}{\partial x}\frac{\partial N_m}{\partial x} + \frac{\partial C}{\partial y}\frac{\partial N_m}{\partial y}\right), \tag{8d}$$
$$\frac{\mu_{nf}}{\mu_f}Pr\nabla^2\omega = \frac{\rho_{nf}}{\rho_f}\left(u\frac{\partial\omega}{\partial x} + v\frac{\partial\omega}{\partial y}\right) - RaPr\left(\frac{(\rho\beta)_{nf}}{\rho_f\beta_f}\frac{\partial T}{\partial x} - Rb\frac{\partial N_m}{\partial x}\right) - Mn_F Pr\left(\frac{\partial H}{\partial x}\frac{\partial T}{\partial y} - \frac{\partial H}{\partial y}\frac{\partial T}{\partial x}\right) + \frac{\sigma_{nf}}{\sigma_f}Ha^2 Pr\Big[H_x^2 v_x - H_x H_y(u_x - v_y) - H_y^2 u_y + 2H_x H_{xdx} v - H_{xdx}H_y u - H_x H_{ydx} u - 2H_y H_{ydy} u + H_{xdy}H_y v + H_x H_{ydy} v\Big], \tag{8e}$$

where $H_{xdx}, H_{xdy}, H_{ydx}, H_{ydy}$ are partial derivatives of $H_x = |y_{ms}|\frac{y - y_{ms}}{(x-x_{ms})^2 + (y-y_{ms})^2}$ and $H_y = |y_{ms}|\frac{x_{ms} - x}{(x-x_{ms})^2 + (y-y_{ms})^2}$, and $H = \sqrt{H_x^2 + H_y^2}$. The nondimensional parameters are Prandtl, Hartmann, Rayleigh, bioconvection Rayleigh, Lewis, Peclet and magnetic numbers given as

$$Pr = \frac{\nu_f}{\alpha_f},\ Ha = L\mu_0 H_0\sqrt{\frac{\sigma_f}{\mu_f}}, Ra = \frac{g\beta_f L^3\Delta T}{\alpha_f\nu_f}, \tag{9a}$$
$$R_b = \frac{\gamma\Delta\rho n_0}{\rho_f\beta_f\Delta T},\quad Pe = \frac{\tilde{b}W_c}{D_n},\quad Le = \frac{\alpha_f}{D_c},\quad Mn_F = \frac{\mu_0 H_0^2\tilde{K}\Delta T L^2}{\mu_f\alpha_f} \tag{9b}$$

where ν is the kinematic viscosity, g is the gravitational acceleration, γ is the mean volume of microorganism, D_c is the diffusivity of oxygen concentration, W_c is the maximum cell swimming speed, $\tilde{b}$ is the chemotaxis constant, D_n is the diffusivity of microorganism, L is the characteristic length, n_0 is the average density of bacteria, μ_0 is the magnetic permeability, H_0 is the intensity of the magnetic field, $\tilde{K}$ is a constant, ΔT is the temperature difference and $\Delta\rho = \rho_{cell} - \rho_{nf}$.

III. COMPUTATIONAL APPROACHES

A. Radial Basis Function (RBF) Method

The numerical part of the study utilizes the RBF collocation method to compute spatial derivatives.

RBFs are functions depending on the radial (Euclidean) distance r between the collocation (x_j, y_j) and the field (x, y) points [19], [20].

Any unknown φ may be written as a product of a coordinate matrix R constructed by an RBF and an unknown vector of coefficients. The partial derivatives of unknown is also easily derived by this product and by the straightforward derivative calculations of RBFs. The differentiation matrices for x-, y- derivatives and Laplacian are found as

$$D_x = \frac{\partial R}{\partial x}R^{-1}, D_y = \frac{\partial R}{\partial y}R^{-1}, D_2 = \left(\frac{\partial^2 R}{\partial x^2} + \frac{\partial^2 R}{\partial y^2}\right)R^{-1}, \tag{10}$$

In the current study, a polyharmonic spline $g = r^7$, is employed, using uniformly spaced grid points.

Iterations are terminated if the sum of the relative residuals in infinity norm is less than a tolerance 10^{-5}. A convergence acceleration parameter $\tau (0 < \tau < 1)$ is utilized once ω equation is solved.

Average Nusselt and Sherwood numbers, and density of the bacteria along the heated wall are computed by

$$\overline{Nu} = -\frac{k_{nf}}{k_f}\int_0^1 \frac{\partial T}{\partial x}dy, \quad \overline{Sh} = -\int_0^1 \frac{\partial C}{\partial x}dy,$$
$$\overline{Nm} = -\int_0^1 \frac{\partial N_m}{\partial x}dy, \tag{11}$$

using composite Simpson's rule on uniform grids. The statistical mean of bacteria ($mean(Nm)$) is also evaluated.

B. Neural Network Regression

The process starts with an input layer, followed by one or more hidden layers, and ends with an output layer [21]. Mathematically, this can be represented as:

$$\hat{\mathbf{o}} = f(W\mathbf{x} + b) \tag{12}$$

In this equation, W is the weight matrix, b is the bias vector, $\mathbf{x}$ is the input feature vector, $\hat{\mathbf{o}}$ is the predicted output, and f is the activation function.

In MATLAB, the fitrnet function is used to train a regression neural network. First, the dataset is divided into training and testing sets. The training data is standardized using z-score normalization, and the test data is standardized using the same parameters when it is evaluated through MATLAB's predict function.

The training process uses a feedforward neural network, involving both forward and backward passes. Initially, weights and biases for each layer are randomly initialized. These parameters are then updated through an optimization algorithm that minimizes the mean squared error (MSE) loss using the quasi-Newton method.

This optimization continues until the maximum number of iterations is reached. In the forward pass, the weighted input (including bias) is passed through the ReLU activation function before being sent to the next layer.

The size of each hidden layer refers to the number of neurons it contains, while the total number of hidden layers defines the depth of the network. For instance, a bilayer network has two hidden layers, and a trilayer network has three.

IV. MODELING RESULTS

The the numerical computations are carried out in the set of combination of parameters $Ra \in [10^2, 10^3, 10^4]$, $Rb = [10, 25, 50]$, $Pe = [0.5, 1, 2.5]$, $Ha = [10, 25, 50]$, $Mn_F = [25, 50, 100]$ while $Pr = 6.8$, $\xi = 0.02$ and $Le = 1$ are held fixed. The coordinates of location of magnetic source are also considered in $x_{\rm ms} = [-0.01, -0.04, -0.08]$, $y_{\rm ms} = [0.1, 0.25, 0.5, 0.75, 0.9]$. The inputs are $Ra, Rb, Pe, Ha, Mn_F, x_{\rm ms}, y_{\rm ms}$ and the stored outputs are $\overline{Nu}, \overline{Sh}, \overline{Nm}, mean(Nm)$. The stored data as a matrix is of size 3645×11. The first 7 columns are for inputs, and the last four columns are for outputs.

In Table II, using a data split into 80% train and 20% train sets, NN modeling is checked in different layer sizes and number of hidden layers. At any fixed layer size, both bilayer and trilayer NN result in smaller MSE results than one layer NN. At a fixed number of layers, the rise in layer size gives better prediction results. Because of these good metric results, no more fine-tuning is processed.

TABLE II
NN modeling in different layer sizes and the number of layers in 80:20 partitioned dataset.

Lsz	#	$\overline{Nu}$	$\overline{Sh}$	$\overline{Nm}$	$mean(Nm)$
10	1	6.12e-04	1.52e-05	1.07e-04	7.87e-06
	2	9.38e-05	1.62e-05	7.17e-05	4.88e-06
	3	9.64e-05	1.04e-05	2.30e-05	4.26e-06
25	1	2.10e-04	1.38e-05	5.37e-05	2.98e-06
	2	6.48e-06	5.45e-06	1.51e-05	6.23e-06
	3	2.33e-06	2.23e-06	5.60e-06	2.35e-06
50	1	5.81e-05	7.56e-06	3.28e-05	3.40e-06
	2	3.08e-06	2.72e-06	5.05e-06	1.07e-06
	3	2.23e-06	1.55e-06	2.18e-05	1.24e-06

In Table III, the distinct partitioned sets are controlled. In Target column, the first number shows the percentage for train data and the second number refers to the test data percentage. As can be noted that if the data is trained on a smaller train set (50:50), the MSE metrics are found larger than the case of a larger train set (80:20). That is, the more the data is trained, better predictions are found.

In Figure 2, bilayer NN modeling based on divided data of ratios $80:20$ with 50 layer sizes is presented. The good prediction results close to the perfect prediction lines along the left subplots in the first column of

TABLE III

Different partititoned sets are checked here.

Target	$\overline{Nu}$	$\overline{Sh}$	$\overline{Nm}$	$mean(Nm)$
50 : 50	1.43e-05	4.77e-06	2.53e-05	1.47e-06
60 : 40	3.71e-06	4.34e-06	1.34e-05	1.28e-06
70 : 30	4.65e-06	2.75e-06	1.00e-05	1.22e-06
80 : 20	3.08e-06	2.72e-06	5.05e-06	1.07e-06

figure. In the second column, small residuals of response variables also confirm the good fit.

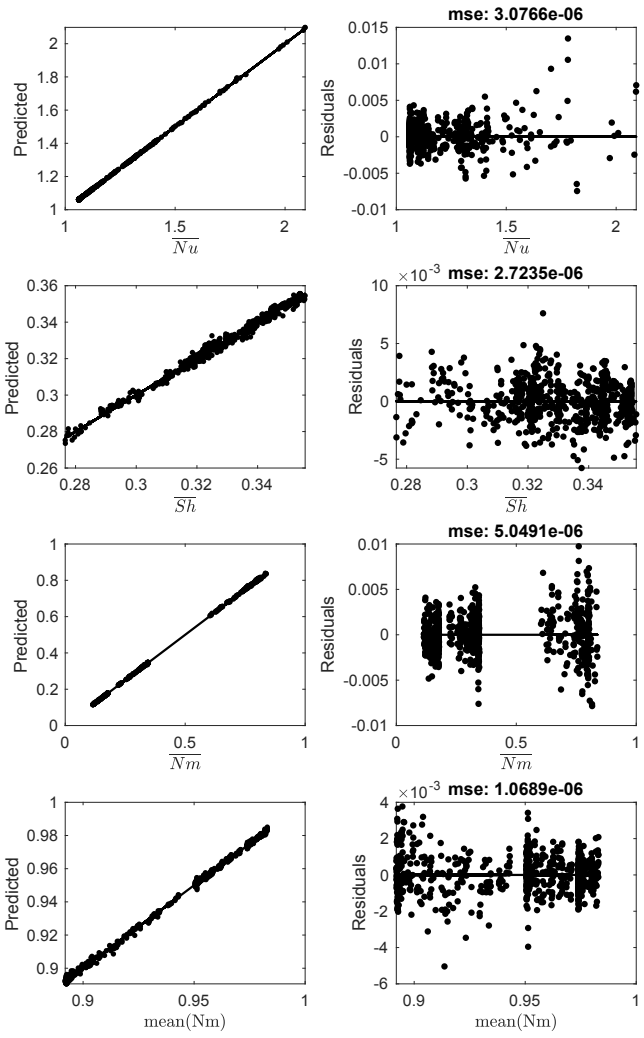

Fig. 2. Bilayer NN modeling with 80 : 20 partitioned data and 50 layer sizes.

More NN analysis is also carried out as is displayed in Fig. 3. In this case, the different number of neurons (10, 25, 50, 75, 100) in different number of layers (1,2,3,4), average MSE outcomes are plotted. As is noted that optimal efficiency occurs at around 50 neurons per layer and at 2-3 hidden layers, balancing model complexity and performance. The performance degrades the number of layers is increased to 4 pointing out a start on overfitting.

This extended analysis confirms that mid-sized networks (50 neurons) with moderate depth (2-3 layers) provide optimal performance for this bioconvection flow problem.

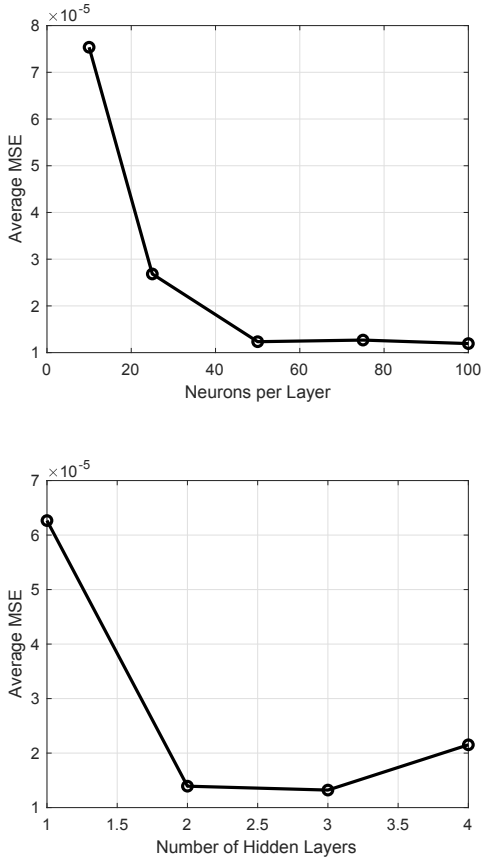

Fig. 3. More analysis on NN modeling with 80 : 20 partitioned data.

V. Physical Interpretations

TABLE IV

Effect of Input Parameters on $\overline{Nu}, \overline{Sh}, \overline{Nm}$

Input	$\overline{Nu}$	$\overline{Sh}$	$\overline{Nm}$	$mean(Nm)$
Ra	↑ 25.13%	↓ 10.78%	↓ 27.64%	↑ 0.63%
Rb	↑ 0.02%	↑ 0.11%	↓ 0.03%	↓ 0.00%
Pe	↑ 0.06%	↓ 9.10%	↑ 353.41%	↓ 8.34%
Ha	↓ 0.06%	↑ 0.15%	↑ 0.54%	↓ 0.01%
MnF	↓ 0.00%	↑ 0.04%	↑ 0.05%	↓ 0.01%
xms	↓ 0.00%	↑ 0.01%	↑ 0.05%	↑ 0.01%
yms	↓ 0.05%	↑ 0.30%	↑ 0.74%	↓ 0.01%

In Table IV, findings show that while the magnetic source position does influence flow characteristics, its effects are modest compared to the primary flow parameters like Rayleigh number and Peclet number. This explains why the neural network model could achieve good

accuracy with relatively simple architectures, as the dominant physical relationships are driven by a few key parameters.

VI. CONCLUSIONS

In this study, an NN model is developed on the Cu-water nanofluid flow including oxytactic bacteria under the impact of point source magnetic field which is located near the hot wall. The governing equations of bioconvection flow problem including magnetic source terms are solved by RBF method to get data set for different values of Rayleigh, bioconvection Rayleigh, Peclet, Hartmann, magnetic numbers and location of magnetic source. In NN process, the average Nusselt and Sherwood numbers, the density and mean value of bacteria are predicted in different layer sizes and numbers. The mean square error is less than 5.1e-6 which indicates that the NN model can estimate the high accuracy. However, we acknowledge that some key parameters such as the Prandtl number, Lewis number, and nanofluid volume fraction are kept constant during dataset generation. This limits the model's generalizability across different fluid types and configurations. In future work, we plan to expand the parameter space and investigate how these variables influence model performance and physical outcomes.

Acknowledgment

This study was supported by TED University Institutional Research Fund (TEDU-IRF).

References

[1] J. O. Kessler, The external dynamics of swimming microorganisms, Progress in Psychological Research, vol. 4, pp. 257-307, 1986.

[2] A. J. Hillesdon, and T. J. Pedley, Bioconvection in suspensions of oxytactic bacteria: linear theory. Journal of Fluid Mechanics, vol. 324, pp. 223-259, 1996.

[3] A. V. Kuznetsov, The onset of thermo-bioconvection in a shallow fluid saturated porous layer heated from below in a suspension of oxytactic microorganisms, European Journal of Mechanics-B/Fluids, vol. 25, pp. 223-233, 2006.

[4] C. S. Balla, C. Haritha, K. Naikoti, and A. M. Rashad, Bioconvection in nanofluid-saturated porous square cavity containing oxytactic microorganisms, International Journal of Numerical Methods for Heat & Fluid Flow, vol. 2 no. 4, pp. 1448-1465, 2019.

[5] N. Biswas, N. K. Manna, D. K. Mandal, and R. S. R., Gorla, Magnetohydrodynamic bioconvection of oxytactic microorganisms in porous media saturated with Cu–water nanofluid, International Journal of Numerical Methods for Heat & Fluid Flow, vol. 31 no. 11, pp.3461-3489, 2021.

[6] N. Biswas, A. Datta, N. K. Manna, D. K., Mandal, and R. S. R. Gorla, Thermo-bioconvection of oxytactic microorganisms in porous media in the presence of magnetic field, International Journal of Numerical Methods for Heat & Fluid Flow, vol. 31 no. 5, pp. 1638-1661, 2021

[7] N. Biswas, N. K. Manna, D. K. Mandal, and R. S. R. Gorla, Magnetohydrodynamic mixed bioconvection of oxytactic microorganisms in a nanofluid-saturated porous cavity heated with a bell-shaped curved bottom, International Journal of Numerical Methods for Heat & Fluid Flow, vol. 31 no. 10, pp. 3722-3751, 2021.

[8] S. Hussain, and B. Pekmen Geridonmez, Mixed bioconvection flow of Ag-MgO/water in the presence of oxytactic bacteria and inclined periodic magnetic field, International Communications in Heat and Mass Transfer, vol. 134, p. 106015, 2022.

[9] A. Shafiq, A. B. Çolak, and T. N. Sindhu, Significance of bioconvective flow of MHD thixotropic nanofluid passing through a vertical surface by machine learning algorithm, Chinese Journal of Physics, vol. 80, pp. 427-444, 2022.

[10] P. Chandra, and R. Das, Finite-element-based machine-learning algorithm for studying gyrotactic-nanofluid flow via stretching surface, International Journal for Numerical Methods in Fluids, vol. 95 no. 12, pp. 1888-1912, 2023.

[11] S. Hussain, F. Ertam, M. B. B. Hamida, H. F. Oztop, and N. H. Abu-Hamdeh, Analysis of bioconvection and oxytactic microorganisms in a porous cavity with nano-enhanced phase change materials and quadrant heater: Application of support vector regression based model, Journal of Energy Storage, vol. 63, p. 107059, 2023.

[12] S. Hussain, H. F. Öztop, A. M. Alsharif, and F. Ertam, Mixed bioconvection of nanofluid of oxytactic bacteria through a porous cavity with inlet and outlet under periodic magnetic field using artificial intelligence based on LightGBM algorithm, Thermal Science and Engineering Progress, p. 102589, 2024.

[13] M. I. U. Rehman, H. Chen, M. I. Khan, A. Hamid, and A. Masmoudi, Modeling and predicting heat transfer performance in bioconvection flow around a circular cylinder using an artificial neural network approach. Tribology International, vol. 200, p. 110182, 2024.

[14] S. M. Sait, R. Ellahi, N. Khalid, T.Taha, and A. Zeeshan, Effects of thermal radiation on MHD bioconvection flow of non-Newtonian fluids using linear regression based machine learning and artificial neural networks. International Journal of Numerical Methods for Heat & Fluid Flow, 2025.

[15] K. Khanafer, K. Vafai, and M. Lightstone, Buoyancy-driven heat transfer enhancement in a two-dimensional enclosure utilizing nanofluids, International Journal of Heat and Mass Transfer, vol. 46, pp. 3639-3653, 2003.

[16] J. M. Garnett, Xii. Colours in metal glasses and in metallic films, Philosophical Transactions of the Royal Society of London. Series A, Containing Papers of a Mathematical or Physical Character, vol. 203, no. 359-371, pp. 385–420, 1904.

[17] H. C. Brinkman, The viscosity of concentrated suspensions and solutions, The Journal of Chemical Physics, vol. 20, no. 4, pp. 571–571, 1952.

[18] M. Ghalambaz, S. A. M. Mehryan, E. Izadpanahi, A. J. Chamkha, and D. Wen, MHD natural convection of Cu–Al2O3 water hybrid nanofluids in a cavity equally divided into two parts by a vertical flexible partition membrane, Journal of Thermal Analysis and Calorimetry, vol. 138, pp. 1723-1743, 2019.

[19] G. E. Fasshauer, Meshfree Approximation Methods with Matlab, World Scientific Publications, Singapore, 2007.

[20] G. E. Fasshauer, and M. McCourt, , Kernel-based Approximation Methods using MATLAB, World Scientific Publications, Singapore, 2015.

[21] T. W.S. Chow, and S.-Y. Cho, Neural Networks and Computing, Imperial College Press, 2007.